# Experimental Study of Transverse Bed Motion in Rotary Kilns

H. HENEIN, J. K. BRIMACOMBE, and A. P. WATKINSON

Slumping and rolling beds have been studied extensively in a continuous pilot kiln and batch rotary cylinders. Solids investigated include nickel oxide pellets, limestone, sand, and gravel. The effect of variables such as rotational speed, bed depth, cylinder diameter, particle size, and particle shape on bed motion has been determined. For a given material, the different modes of bed motion can be delineated conveniently on a Bed Behavior Diagram which is a plot of bed depth *vs* rotational speed. The scaling of bed behavior with respect to particle size and cylinder diameter requires similarity of Froude number modified by $(D/d_p)^{1/2}$, and pct fill. Measurements of key variables characterizing slumping and rolling beds have also been made.

## I. INTRODUCTION

As a rotary kiln turns on its axis the solids bed inside is subjected to transverse motion. Viewing the kiln on end, the bed motion may take on one of many forms—slipping, slumping, rolling, cascading, cataracting, and centrifuging —as shown in Figure 1, depending on such variables as rotational speed, kiln diameter, pct fill, bed/wall friction, and bed particle characteristics. The relationship between bed motion and these variables has not been fully established quantitatively. Moreover, very little is known of the effect of the mode of transverse motion on heat transfer to the bed, mixing within the bed, dust generation, and residence time of the solids in the kiln. One of the few facts widely recognized is that the slipping mode, in which the bed slides against the inside surface of the kiln wall, drastically reduces mixing of the solids and concomitant heat transfer; but the conditions giving rise to bed slippage for a given solid remain only partially understood.

Thus, the purpose of this investigation has been to characterize transverse bed motion quantitatively in terms of the important kiln variables. Both experimental and theoretical approaches have been taken in the study. The experimental work, which is reported in this paper, has focused on determining the conditions leading to slumping and rolling beds most commonly found in rotary kiln operations. As will be seen, the modes of bed motion can be delineated usefully on plots of bed depth *vs* rotational speed (or pct fill *vs* Froude number) which we have termed Bed Behavior Diagrams. The theoretical work, to be described in a following paper, provides a fundamental basis for the slumping/rolling behavior as well as the other modes of bed motion and makes it possible to predict bed behavior quantitatively based on measured particle characteristics and the bed/wall friction coefficient. In both works an attempt has been made to determine scaling criteria in order to scale up laboratory results to industrial-size kilns.

H. HENEIN, formerly Graduate Student, Department of Metallurgical Engineering, The University of British Columbia, is now with the Department of Metallurgical Engineering and Materials Science, Carnegie-Mellon University, Pittsburgh, PA 15213 as Assistant Professor. J. K. BRIMACOMBE, Stelco Professor of Process Metallurgy, Department of Metallurgical Engineering, The University of British Columbia, Vancouver, British Columbia V6T 1W5 Canada. A. P. WATKINSON is Professor, Department of Chemical Engineering, The University of British Columbia, Vancouver, British Columbia V6T 1W5, Canada.

Manuscript submitted August 4, 1982.

## II. DESCRIPTION OF BED MOTION AND PREVIOUS WORK

Of the six modes of transverse bed motion shown in Figure 1 only the first four will be discussed in this section since cataracting and centrifuging are not normally found in rotary kiln operations. The slumping bed has been described by Zablotny,[1] Reuter,[2] Schnabel,[3] and Wahlster *et al.*[4] It resembles an avalanche as a segment of the solids detaches from the bed and slumps toward the lower extremity of the bed surface. The slump occurs periodically each time the bed, rotating upward with the kiln wall, reaches an upper angle of repose, $\phi_R$, of the solids as shown in Figure 1. Following a slump, the bed inclination is lower than the static angle of repose and is given by position BP in Figure 1. The segment of solids slumping (ABC in Figure 1) is defined by a shearing angle, $\gamma$, which has been reported to be 12 to 15 deg at 1 to 2 rpm.[1]

Slumping has been studied previously by measurement of the slumping frequency,[1,2,4,5] the angle of repose of the solids,[4] and the residence time of particles on the surface of the bed.[4] Reported measurements of the slumping frequency are contradictory with respect to the effect of the physical properties of the bulk solids.[1,4] However, there is general agreement that the slumping frequency increases with increasing rotational speed of the cylinder;[2,4,5] and Pearce[5] reported the following relationship based on observations of several industrial kilns*

*Symbols are defined at the end of the paper.

$$S = \frac{60}{t_s} + \frac{24}{n} \qquad [1]$$

More recently Reuter[2] found that the slumping frequency depended on the ratio $n/n_c$ ($n_c = (30/\pi)\sqrt{2g/D}$ for small particles). The angle of repose of the bed does not change with increasing rotational speed according to Wahlster *et al*[4] who also found that the ratio of particle residence time on the bed surface to the bulk circulation time is in the range of one-twelfth to one-fifth.

At higher rotational speeds, the periodic slumping of the bed gives way to rolling,[2,4] which is characterized by the continuous motion of a layer of solids over the bed surface. This rolling zone is continually fed with solids from the bulk of the burden, which reach the upper part of the bed by means of the kiln rotation. The rolling bed, at low rotational

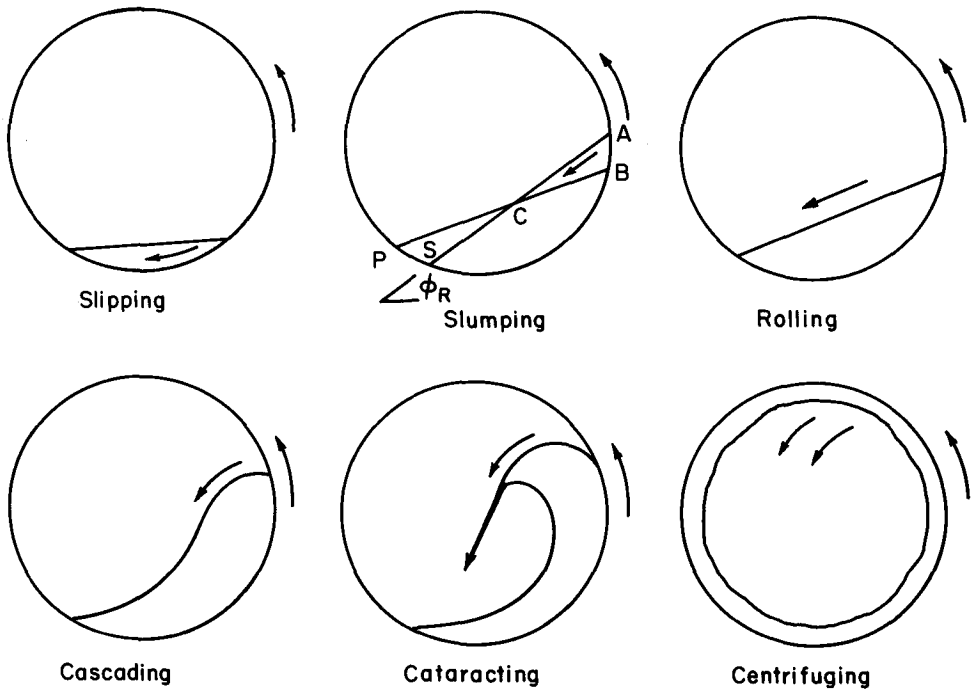


Fig. 1 — Schematic diagram showing modes of transverse bed motion.

speeds, assumes a constant angle of inclination and a flat planar surface. But with increasing speed, the solids in the upper corner, or apex, of the bed ride higher up the wall before detaching such that the cross-section of the bed assumes a crescent or kidney shape. This is the cascading mode of bed motion (Figure 1).

Quantitative characterization of a rolling or a cascading bed has been attempted by measuring the bed inclination,[2,4,6,7-10] the residence time of solids on the surface,[2,11] the thickness of the active rolling layer,[2] and the conditions under which bed behavior changes from slumping to rolling.[4,7,12,13] The inclination of a rolling bed (close to the point of slumping) is thought to be the dynamic angle of repose of the bulk solids. Rutgers,[7] Reuter,[2] and Ronco[8] have compared the dynamic and static angles of repose and reported the former to be higher. However, Franklin and Johanson[9] have found the opposite which is in line with the basic principles of mechanics.[10] The bed inclination is not influenced by increasing rotational speed according to Wahlster *et al*;[4] but Wes *et al*[6] have found the inclination to decrease with increasing speed, probably due to the presence of protrusions in their cylinder. The residence time of particles on the surface of a rolling bed has been measured by Reuter[2] and Oyama,[11] but their data are not in a usable form for bed-motion characterization. Other bed surface measurements of Reuter[2] indicate an increase in the active-layer depth with increasing rotational speed and a smaller increase in the ratio of the active-layer thickness to bed depth with increasing pct fill. Several observers have recorded the operating conditions under which bed motion changes from slumping to rolling. Davis[12] stated that this change was due to the inertia of the particles as well as to the centrifugal force acting on them. However, Rutgers[7] reported that the change in bed behavior occurs at a rotational speed that is one-tenth that of the critical value for centrifuging, $n_c$. Carley-Macauly and Donald[13] claim that this transition occurs at even lower values, 0.056 $n_c$. These correspond to a ratio of centrifugal to gravitational forces of 0.01 and 0.003, respectively. Clearly, the centrifugal force is negligible. The most thorough study of the slumping-rolling transition in bed behavior is that of Wahlster *et al*[4] who found that as the pct fill increased, the critical rotational speed at which the bed behavior changed decreased. For small particle sizes the critical speed increases with increasing size until a maximum is reached at 2 to 4 mm ($d_p/D = 4.4 \times 10^{-3}$ to $8.9 \times 10^{-3}$) after which the critical speed decreases. The type of material was not observed to affect this critical rotational speed.

Three types of slipping motion have been observed,[7,8,14,15] the difference between them being the motion of the bed relative to the rotating kiln wall. In the first type, the solids move upward with the wall to an inclination less than their angle of repose for slumping, then slide downward against the wall, after which the process repeats itself. In the second case the bed moves upward with the wall but at a lower rotational speed, and solids at the top of the bed roll slowly down the inclined surface. Finally, within a particular range of rotational speeds and pct fill, the bed takes up a stationary position as the solids continuously slide against the rotating wall. The investigators cited earlier, together with Rose,[16] all report that little transverse solids mixing takes place in a slipping bed.

From the literature it would appear that slumping beds are most suitably characterized by the static angle of repose of the solids and slumping frequency while rolling beds are best characterized by the active layer thickness on the bed surface and the critical rotational speed for slumping-rolling transition. Such measurements are reported in this paper.

## III. EXPERIMENTAL

A total of ten materials, listed in Table I, were studied. Bed behavior was investigated in the UBC pilot kiln and three shorter rotating cylinders while bed-wall static friction was measured in a separate apparatus.

**Table I. Summary of Results for the Particle Characterization of the Materials Studied**

| Material | Average Size (mm) | Particle Shape | Particle Density ($kg/m^3$) | Loose Bulk Density ($kg/m^3$) | Dense Bulk Density ($kg/m^3$) | Loose Void Fraction | Dense Void Fraction | Static Angle of Repose (Degrees) |
|---|---|---|---|---|---|---|---|---|
| Gravel | 3.0 | Angular | 2870 | 1560 | 1690 | 0.46 | 0.41 | 40.7 |
| Iron Oxide | 11.6 | Spherical | — | — | — | — | — | 31.5 |
| Limestone B | 4.3 | Irregular | 2700 | 1450 | 1610 | 0.46 | 0.40 | 40.3 |
| Limestone C | 1.5 | Irregular | 2690 | 1520 | 1600 | 0.43 | 0.40 | 37.8 |
| Limestone D | 0.58 | Irregular | 2680 | 1490 | 1570 | 0.44 | 0.41 | 35.6 |
| Limestone E | 0.54 | Equidimensional | 2670 | 1680 | 1860 | 0.37 | 0.30 | 38.6 |
| Limestone F | 8.1 | Angular | 2690 | — | — | — | — | 42.8 |
| Nickel Oxide | 4.9 | Spherical | — | 870 | 900 | — | — | 32.5 |
| Sand B | 0.50 | Nodular | 2660 | 1640 | 1740 | 0.38 | 0.35 | 33.4 |
| Sand C | 0.23 | Nodular | 2730 | 1710 | 1810 | 0.37 | 0.34 | 32.2 |

Sand A was very similar to Sand B but contained 5 wt pct -60 mesh fines.

### A. *Particle Characterization*

The materials were characterized by measuring or identifying the following properties: particle size, particle shape, bulk density, apparent particle density, void fraction, and static angle of repose. The particle-size distribution of the ten materials is shown in Figure 2; and the average particle size is presented in Table I together with the other properties. The size analysis was conducted in accordance with standard procedures.[17,18] From Figure 2 the materials are seen to have a narrow size distribution with the exception of Sand C which displayed a multimodal distribution.[19,20,21] Only nickel oxide and Limestone F appear to have log-normal distributions. The plots of log-normal distribution for the other materials indicate they resulted from a coarse size separation process. This was confirmed for the limestone and gravel by the respective suppliers. The particle shape was characterized qualitatively in accordance with the British Standard 2955[22] rather than the classification proposed by Hausner for powdered metals.[23] Observations of the particles before and after tumbling in the rotating cylinders showed no detectable degradation or change in particle shape. The bulk density of the materials was measured with containers having a diameter 50 to 100 times that of the average solids particle size to minimize wall effects.[24] Thus, two 285 mm diameter containers were employed for all but the iron oxide and Limestone F since their wall effects would have been significant. Several measurements of random-loose and random-dense bulk densities were made for each material; the averaged results are listed in Table I. The apparent particle densities were measured using a pycnometric technique in a 1 liter volumetric flask. The void fraction then was calculated as follows:

$$\varepsilon = 1 - \left(\frac{\rho_B}{\rho_p}\right) \qquad [2]$$

The static angle of repose of the materials has been measured using the fixed cone method which, according to Richards and Brown,[25] is preferable to the tilting box and rotating cylinder techniques.

### B. *Rotary Vessels*

As mentioned earlier, both a pilot rotary kiln with continuous feeding and three batch rotating cylinders were employed to observe bed behavior. The pilot kiln, which has been described previously in detail by Brimacombe and Watkinson,[26] is refractory lined, has end dams, and has dimensions of 0.41 mm diameter × 5.5 m; the inclination, rotational speed, and solids feed rate are all variable. A meter rule welded perpendicularly to a long horizontal pipe was introduced axially into the kiln to measure the bed depth along the kiln length.

The dimensions of the three batch cylinders are presented in Table II. Note that cylinders A and B have the same

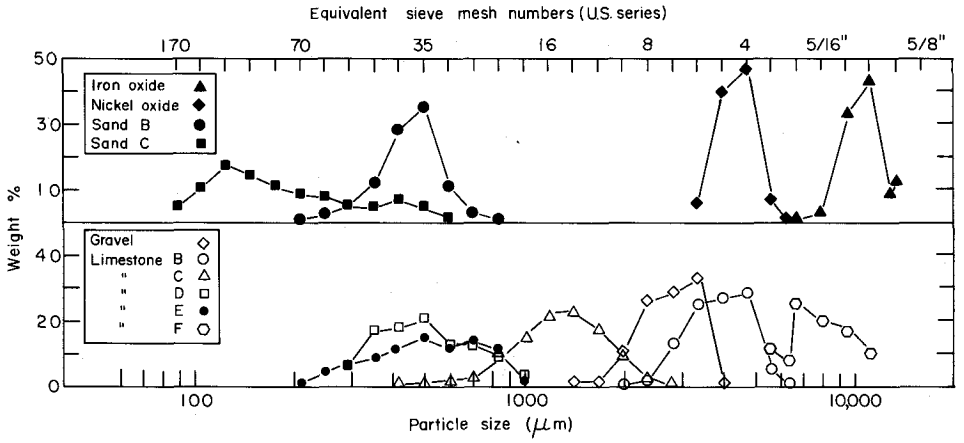


Fig. 2—Particle-size distribution of materials studied.

**Table II. Dimensions of Rotary Vessels**

| Vessel | Inside Diameter (m) | Length (m) |
|---|---|---|
| Pilot kiln | 0.4 | 5.5 |
| Cylinder A | 0.4 | 0.46 |
| Cylinder B | 0.4 | 0.86 |
| Cylinder C | 1.0 | 0.41 |

internal diameter as the pilot kiln. To ensure a high friction coefficient between the cylinder wall and the solids, a 24-3 grit Type E silicon carbide abrasive paper was glued to the inside wall of the three cylinders. One of the two end plates fastened to each cylinder was made of plexiglas, thereby enabling the cross-section of the bed to be viewed and photographed. A hole was cut in the center of the end plates to permit easy access to the solids bed. The rotary cylinders were supported horizontally on two friction rolls one of which was driven by a 1/6 HP electric motor. The maximum rotational speed was about 7 rpm for Cylinders A and B as measured directly using a tachometer with an accuracy of 0.05 rpm.

### C. *Solids-Wall Friction*

The solids-wall friction coefficient was measured by adapting the method of Conrad *et al.*[27] The coefficient of static friction, $\mu_{w/s}$, is given by the tangent of the slipping angle between solids and wall. This angle was measured in an experimental apparatus which consisted of a flat wooden board to which the same abrasive paper used for the inside surface of the rotary cylinders was secured. The granular materials of interest were epoxied onto a cardboard backing and pressed against the abrasive paper by a small weight to ensure good contact. The board was raised by a variable speed electric motor at a maximum lifting rate of 0.17 m per minute until the granular solids slipped. The angle of inclination of the board was measured to within 0.5 deg. The average slipping angles of the different materials are given in Table III. Note that the values are greater than the static angles of repose listed in Table I for each material, respectively.

### D. *Bed Behavior*

In the pilot kiln operating continuously, bed behavior—slumping, rolling, transitional, or slipping—was determined visually under a given set of conditions. The kiln variables studied were the feed rate, rotational speed, inclination of the kiln, and height of discharge dam. All of these variables influence the bed depth profile which was measured in each experiment with the rule described earlier.

In the batch rotary cylinders, bed behavior was studied predominantly using a Light Reflection Distance Gauge (henceforth referred to as an IR sensor). The instrumented technique has advantages of better reproducibility and of providing a permanent record as compared to simple visual observation, and gives information on bed behavior in a more convenient form than is obtained by cinematography. The instrument consisted of an infrared device which emits infrared signals and detects those reflected from the surface at which it is aimed. The current output from the IR sensor was proportional to the distance between the sensor and the surface. Thus, a slumping bed with a constantly changing bed inclination yielded an oscillating signal while a rolling bed resulted in a signal of lower amplitude and irregular period.

**Table III. Measured Angles of Slip of the Materials against the Wall**

| Material | Angle of Slip (Degrees) | Standard Deviation (Degrees) | Number of Observations |
|---|---|---|---|
| Gravel | 48.8 | 1.2 | 5 |
| Iron Oxide | 38.9 | 2.9 | 8 |
| Limestone B | 43.9 | 1.6 | 8 |
| Limestone C | 43.2 | 2.4 | 8 |
| Limestone D | 40.9 | 1.3 | 8 |
| Limestone F | 43.3 | 1.9 | 8 |
| Nickel Oxide | 41.2 | 2.3 | 8 |
| Sand B | 38.8 | 1.1 | 8 |

For an experiment, the sensor was mounted in an acrylic tube above the upper part of the bed surface in the freeboard of the rotating cylinder as shown in Figure 3. The output signal obtained was amplified and fed to a chart recorder. A sample output can be seen in Figure 4. The roughness of the bed surface due to individual particles did not adversely affect the sensor output signal except when the largest particle sizes—Limestone F and iron oxide—were used. For all other materials the effects of surface roughness were less than the changes in bed inclination resulting from a slump.

The reliability of the sensors in determining the transition in bed behavior between slumping and rolling was checked against visual observations for Limestone B and nickel oxide in Cylinder A (Table II). As will be seen, the agreement was quite acceptable. Also, checks were made to determine if the position of the sensor relative to the top of the bed had any influence on the measured transition in bed behavior. The position was found to be unimportant, and normally the sensor was aimed at the upper surface of the bed.

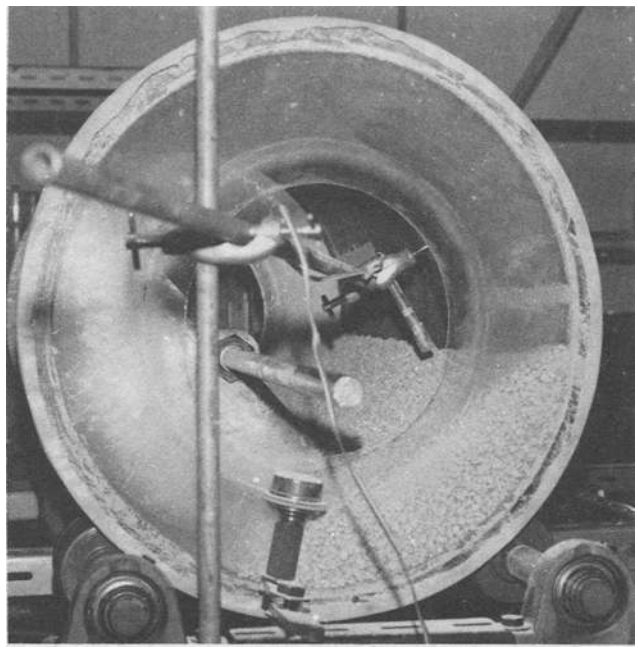

Fig. 3—Photograph showing the position of the IR sensor in one of the rotating cylinders.

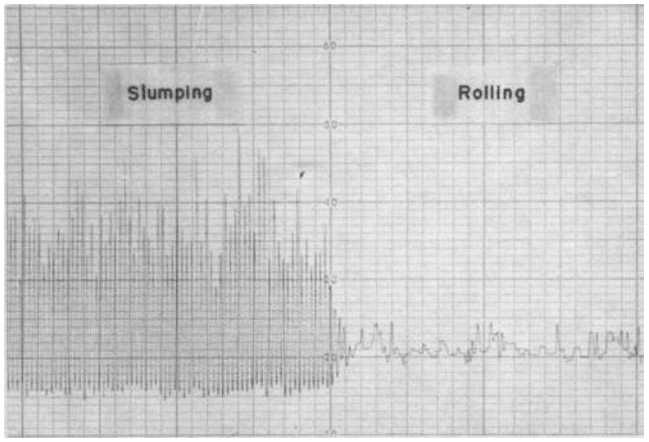


Fig. 4—Sample output from IR sensor for slumping and rolling beds.

### E. *Bed Angles*

Two of the variables measured to characterize the slumping bed were the maximum angle of bed inclination just before a slump occurs and the shear angle. The latter is the angle, relative to horizontal, of the shear plane separating the slumping solids on the bed surface from the material beneath moving with the cylinder wall. The position of the shear plane has been observed to be fixed in space during a slump and to coincide with the final bed inclination once the slumping solids have come to rest. The rolling bed was characterized in part by measurement of the dynamic angle of repose formed by the bed in relation to horizontal. All three angles were measured with a long arm protractor viewing the bed through the plexiglas endplate of the rotary cylinder.

**Table IV. Bed Behavior of Sand A in Pilot Kiln (Kiln Inclination = 1.2 Deg)**

| Run No. | Rotational Speed (r/min) | Axial Distance from Solids Discharge (m) | Local Bed Depth (m) | Feed Rate (kg/h) | Dam† | Bed Behavior |
|---|---|---|---|---|---|---|
| 19 | 0.5 | 0.7 | 0.085 | 29 | A | Transition* |
| 21 | 0.5 | 5.2 | 0.085 | 61 | A | Transition |
| 21 | 0.5 | 0.9 | 0.102 | 61 | A | Transition |
| 34 | 0.5 | 1.5 | 0.103 | 38 | B | Transition |
| 14 | 1.0 | 5.2 | 0.030 | 38 | C | Slumping |
| 18 | 1.0 | 2.0 | 0.032 | 32 | A | Slumping |
| 16 | 1.0 | 5.2 | 0.045 | 67 | C | Slumping |
| 18 | 1.0 | 1.5 | 0.045 | 32 | A | Slumping |
| 18 | 1.0 | 1.2 | 0.054 | 32 | A | Transition |
| 20 | 1.0 | 2.4 | 0.054 | 69 | A | Transition |
| 35 | 1.0 | 5.2 | 0.055 | 79 | B | Transition |
| 18 | 1.0 | 0.9 | 0.064 | 32 | A | Transition |
| 20 | 1.0 | 1.8 | 0.064 | 69 | A | Transition |
| 27 | 2.0 | 1.5 | 0.025 | 29 | A | Rolling |
| 45 | 2.0 | 1.1 | 0.025 | 94 | B | Rolling |
| 46 | 2.0 | 1.1 | 0.025 | 100 | B | Rolling |
| 45 | 2.0 | 1.5 | 0.029 | 94 | B | Rolling |
| 46 | 2.0 | 2.1 | 0.029 | 100 | B | Rolling |
| 28 | 2.0 | 2.1 | 0.032 | 68 | A | Rolling |
| 45 | 2.0 | 2.0 | 0.032 | 94 | B | Rolling |
| 27 | 2.0 | 1.2 | 0.038 | 29 | A | Rolling |
| 28 | 2.0 | 1.8 | 0.038 | 68 | A | Rolling |
| 45 | 2.0 | 2.9 | 0.038 | 94 | B | Rolling |
| 27 | 2.0 | 0.9 | 0.051 | 29 | A | Rolling |
| 28 | 2.0 | 1.2 | 0.051 | 68 | A | Rolling |

*Transition between slumping and rolling
†Height of dams, respectively, were—A: 7 cm, B: 10 cm, C: 4.6 cm. Length of dams was roughly 60 cm while peak height was the following distance from the discharge end—A: 30 cm, B: 50 cm, C: 40 cm.

## IV. RESULTS AND DISCUSSION

### A. *Bed Behavior*

*Pilot Kiln.* In the pilot kiln two or three modes of bed behavior were frequently observed at different axial positions due to changing bed depth. Some of the observations of Sand A for different operating conditions are shown in Table IV. Thus it is seen that for a range of feed rates and dam heights, the bed behavior of Sand A at a given axial location in the kiln depends solely on rotational speed and local bed depth. The same was found for Limestone A when the angle of the kiln inclination was varied; and hence there do not appear to be any downstream effects. This result can be seen more clearly if all of the observations of bed motion involving Sand A in the pilot kiln are presented in a Bed Behavior Diagram which, as mentioned earlier, is a plot of bed depth (or pct fill) *vs* rotational speed (or Froude number). This diagram is shown in Figure 5 where regions of slumping, transition,* rolling, and slipping motion are delineated. Individual observations of local bed motion are observed to be self-consistent in terms of the effect of local bed depth and rotational speed on bed behavior. Slumping predominates at the lowest rotational speeds, less than 0.3 rpm, and slipping occurs at low bed depths, less than 30 mm. The transition between slumping and rolling depends on both bed depth and rotational speed—deeper beds roll at lower speeds.

*The term "transition" is used to describe a bed that exhibits both slumping and rolling behavior.

*Batch Rotary Cylinders.* Because bed behavior for a given material depends uniquely on rotational speed and bed depth (as well as material properties and bed/wall friction), it follows that a batch cylinder can be employed to study bed motion. To check this deduction, a series of bed observation experiments was conducted using Sand A and Cylinder A which has the same ID as the pilot kiln (Table II). The bed depth and rotational speed were varied over the same range as obtained in the pilot kiln. The regions of bed behavior are delineated in Figure 6 and compared to those determined from the pilot kiln (dashed lines). Excellent agreement between batch cylinder and pilot kiln is seen for the slumping-transition boundary, but the comparison is less satisfactory for the transition-rolling boundary, the beds in the pilot kiln taking on a rolling motion at slightly lower rotational speeds than in the cylinder. This difference, which is most pronounced at greater bed depths, arises because thermocouples protruding through the wall into the pilot kiln disturb the bed as they rotate through it and initiate rolling at lower rotational speeds than otherwise would be required. Also, slipping was not observed with Sand A in Cylinder A because its wall was rougher than that of the pilot kiln.

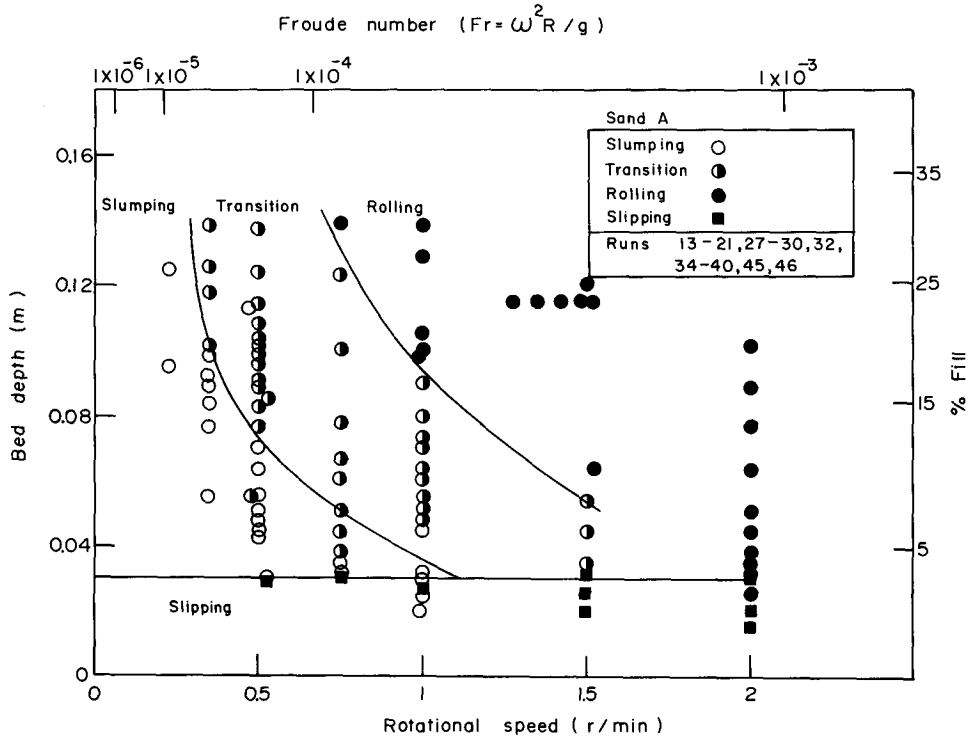


Fig. 5—Bed Behavior Diagram for Sand A visually determined in the UBC pilot kiln.

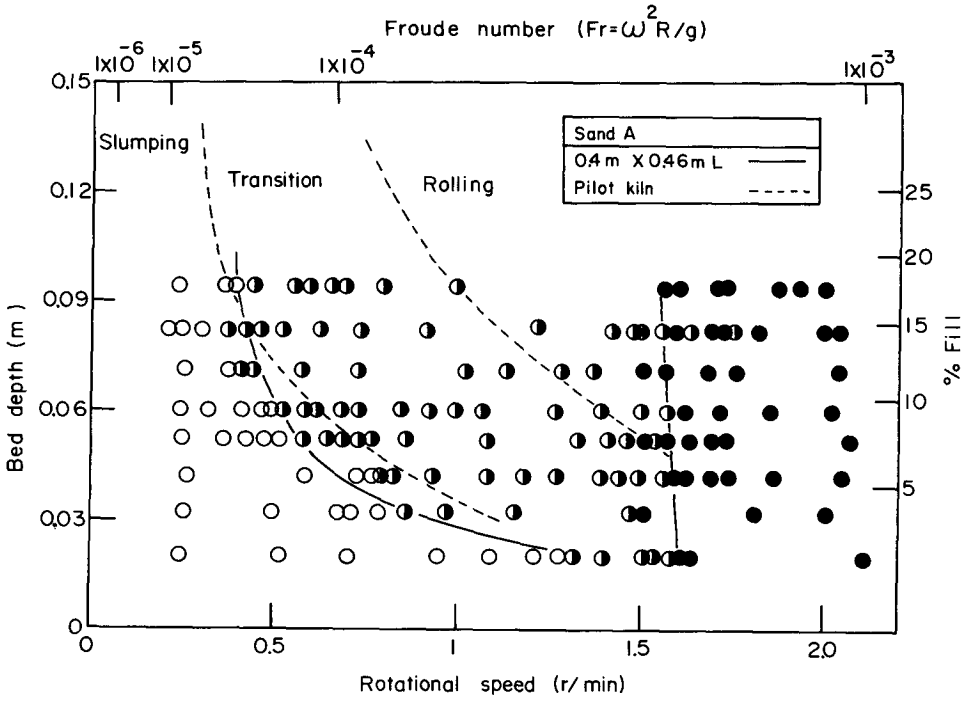


Fig. 6—Bed Behavior Diagram for Sand A visually determined in Cylinder A (0.4 m ID × 0.46 m) and compared to that obtained in the pilot kiln.

Based on this comparison and others, the remainder of bed behavior observations was made using the batch rotary cylinders each equipped with an IR sensor.

*End-Wall Effects.* End-wall effects were investigated by placing two IR sensors in Cylinder A, one close to the end-wall and the other at the axial center. It was found that the solids close to the end-walls tended to roll at lower rotational speeds than those located at the axial midpoint due to the lifting action of the walls. To check this effect further, the motion of beds of Limestone B in Cylinders A and B, having length/diameter ratios of 1:1 and 2:1, respectively, was compared. With the IR sensor located at the axial center of each cylinder, the bed behavior shown in Figure 7 was obtained. The agreement between the two sets of results is satisfactory, although the slumping-transition boundary is found at slightly lower rotational speeds with the shorter cylinder indicating a small influence of the end-walls. Thus, Cylinder A, with a sensor positioned at the axial center of

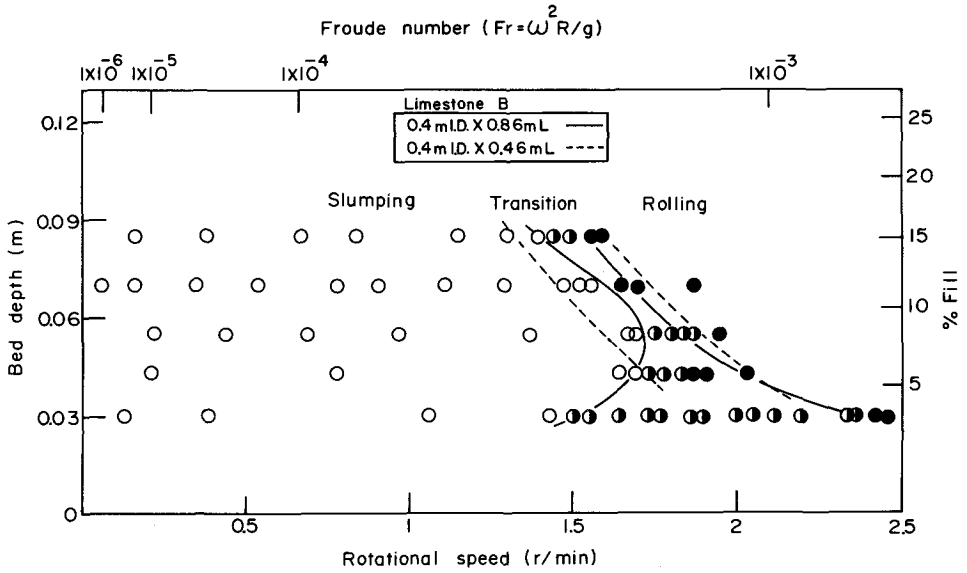


Fig. 7—Bed Behavior Diagram for Limestone B comparing the results from Cylinder A (0.4 m ID × 0.46 m) and Cylinder B (0.4 m ID × 0.86 m).

the cylinder, was employed for the remaining bed motion experiments in which the effect of particle shape, particle size, static angle of repose, and diameter of rotary cylinder on bed behavior was studied. The density of the solids tested was also varied by at least a factor of 2, but no effect on bed behavior and slumping frequency was observed.

*Particle Shape.* As can be seen in Table I, the nickel oxide and Limestone B have roughly the same particle size, 4.9 and 4.3 mm, respectively, but very different shapes, spherical *vs* irregular. The Bed Behavior diagrams for these materials, turned in Cylinder A, are shown in Figures 8 and 9. Thus, the slumping-transition-rolling boundaries occur at much lower rotational speeds for the nickel oxide spheres than the irregular limestone particles, as would be expected. The bed motion boundaries for both materials exhibit a dependence on bed depth. Also note that the boundaries have been determined both visually and with the IR sensors; and there is reasonable agreement.

The influence of the shape of smaller particles can be seen by comparing the bed behavior of Limestone D (0.58 mm, irregular) with that of Sand B (0.50 mm, nodular). The Bed Behavior Diagrams for the two materials are shown in Figures 10 and 11, respectively. Again, the bed motion boundaries are found at lower rotational speeds for the more spherical particles, Sand B. The greater ease with which the spherical and nodular particles roll is consistent with experience and general observations on the flowability of granular materials in bins and hoppers.[25,28,29]

*Particle Size.* The effect of particle size on bed behavior can be assessed by comparing Limestones B and D. According to Table I, the limestones have the same irregular particle shape but quite different sizes, 4.3 mm for B and

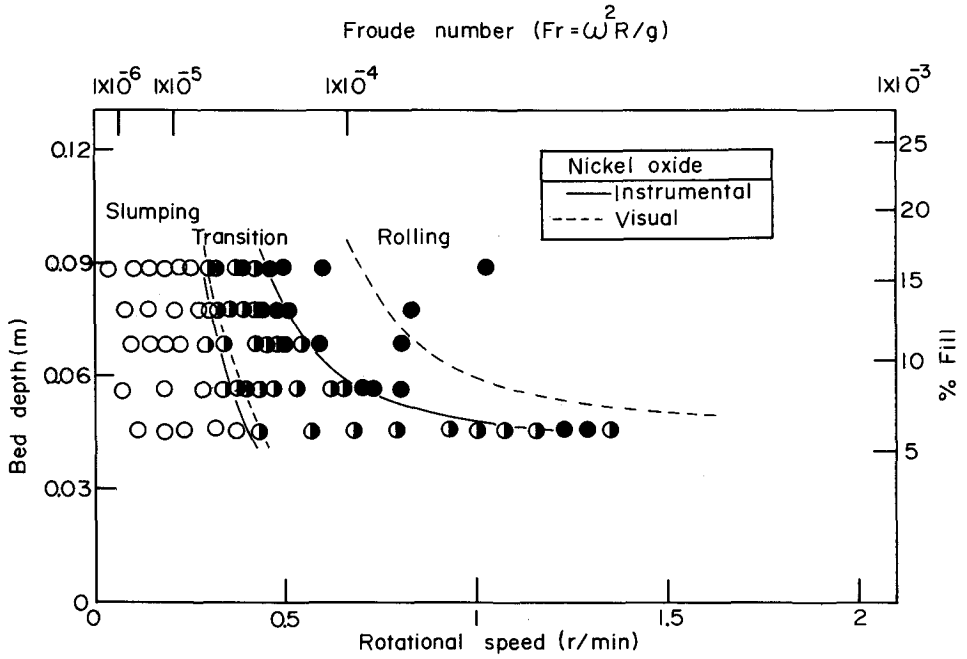


Fig. 8—Bed Behavior Diagram for nickel oxide in Cylinder A.

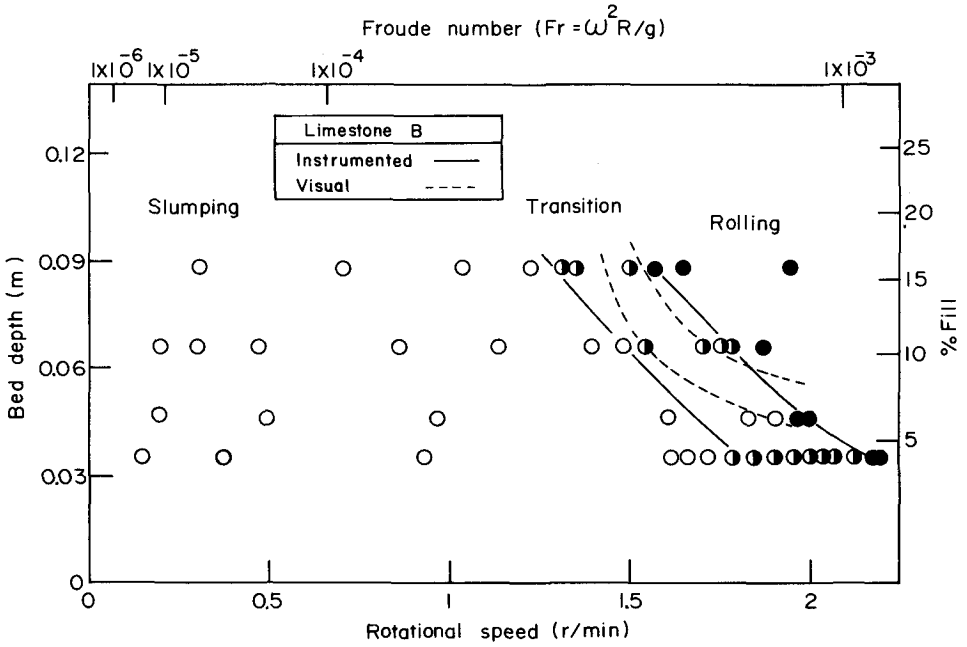


Fig. 9—Bed Behavior Diagram for Limestone B in Cylinder A.

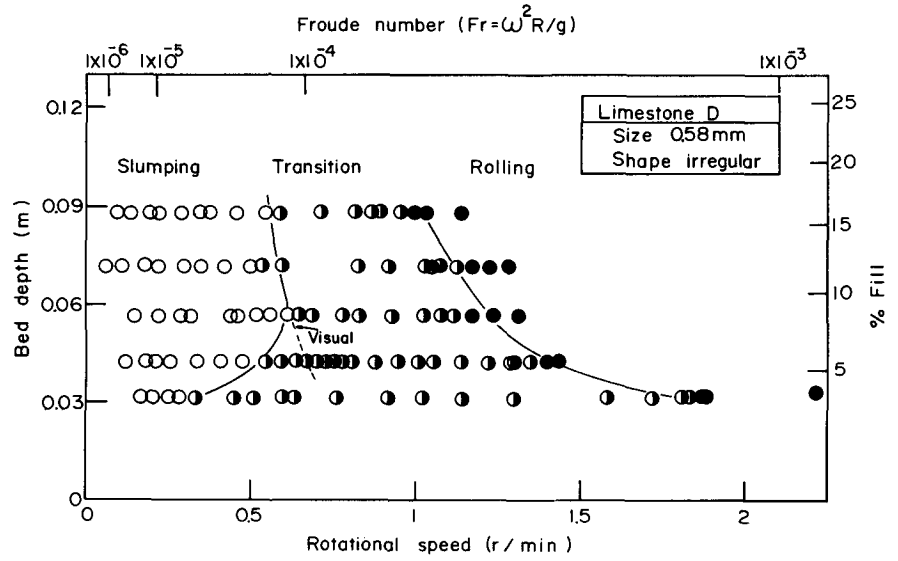


Fig. 10—Bed Behavior Diagram for Limestone D in Cylinder A.

0.58 mm for D. From the Bed Behavior Diagrams, shown in Figures 9 and 10, the smaller Limestone D is seen to roll at lower rotational speeds (and Froude numbers) and also to exhibit a larger transition zone. To illustrate further the particle size effect, a Bed Behavior Diagram, presented in Figure 12, was determined experimentally for Limestone C which has the same irregular particle shape as B and D but an intermediate particle size of 1.5 mm. The bed motion boundaries seen in Figure 12 fall between those for Limestones B and D, and moreover show a bed depth dependency which is in agreement with the observations of Wahlster *et al.*[4]

*Static Angle of Repose.* Examination of the Bed-Behavior Diagrams (Figures 8 through 12 presented earlier and Figure 13 shown for gravel), in the light of the static angles of repose of the materials (Table I), reveals a clear trend, as might be expected. To within experimental error, materials with smaller angles of repose, or greater flowability, generally have bed motion boundaries at lower rotational speeds, *i.e.*, roll more easily. Thus, the static angle of repose, which incorporates effects of particle shape and size, provides a reliable guide to the relative position of slumping-rolling boundaries for different materials.

*Diameter of Rotary Cylinder.* To evaluate the effect of cylinder diameter on bed behavior, measurements were made of the motion of Limestone B in Cylinder C which has a diameter 2.5 times greater than that of Cylinder A. The resulting Bed Behavior Diagram is shown in Figure 14 and can be compared to results obtained in the smaller cylinder, seen earlier in Figure 9. Thus, the transition from slumping to rolling for a given pct fill occurs at lower values of rotational speed and Froude number in the larger cylinder. Note also that in both cylinders, bed motion is dependent on bed depth.

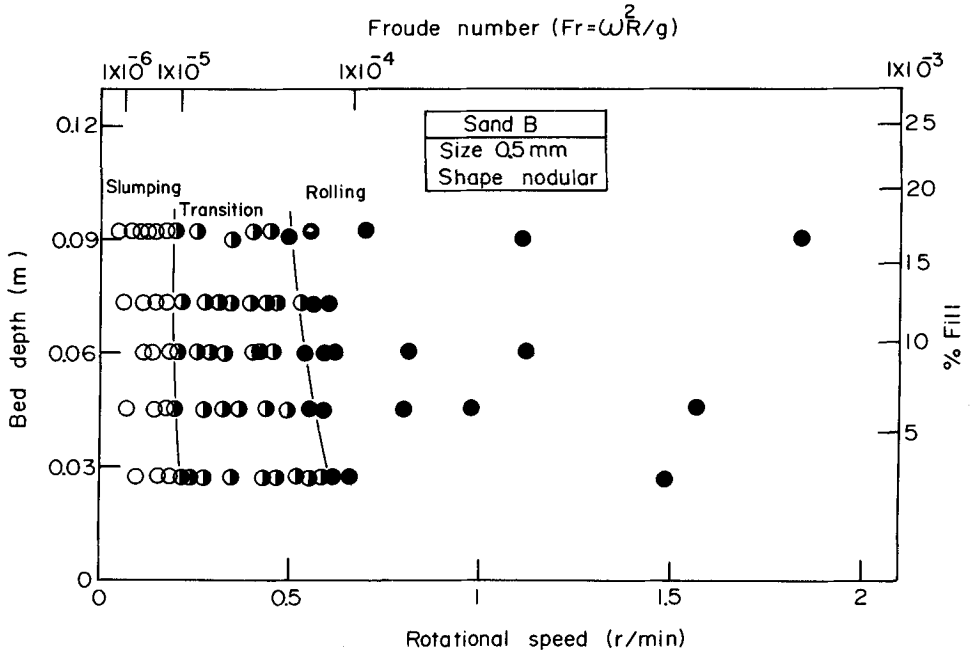


Fig. 11 — Bed Behavior Diagram for Sand B in Cylinder A.

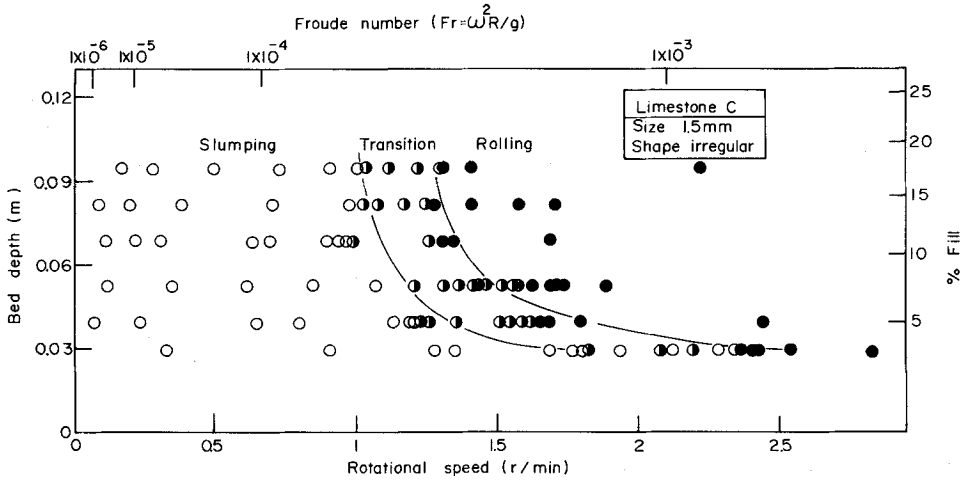


Fig. 12 — Bed Behavior Diagram for Limestone C in Cylinder A.

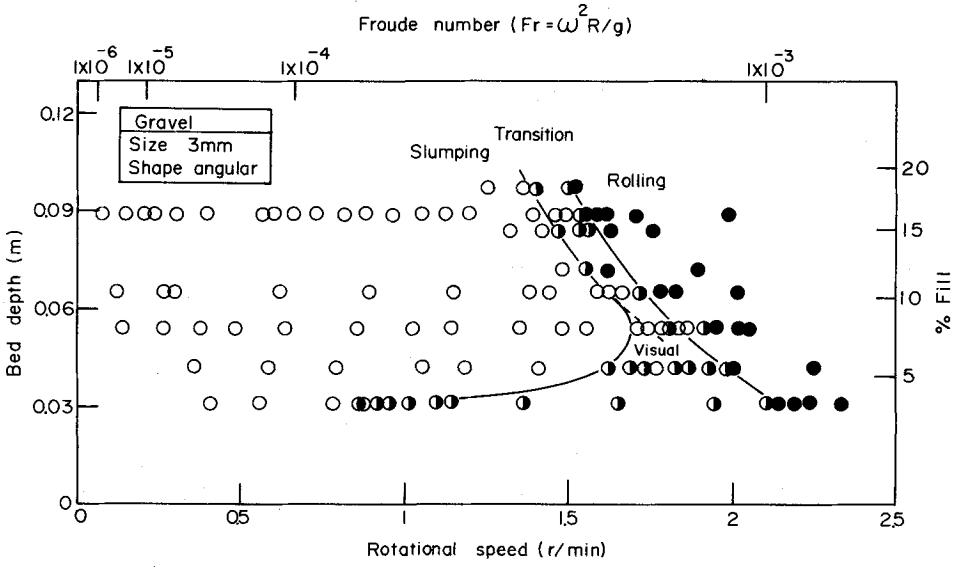


Fig. 13 — Bed Behavior Diagram for gravel in Cylinder A.

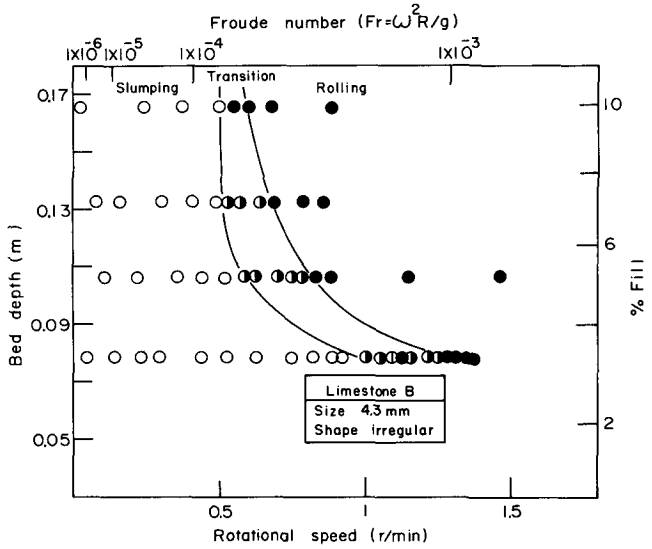


Fig. 14—Bed Behavior Diagram for Limestone B in Cylinder C (1.06 m ID × 0.4 m).

*Scale-Up.* From the preceding sections, it is apparent that Froude number and pct fill, by themselves, do not characterize bed behavior for a given material. Particle size (Figures 9, 10, and 12) and cylinder diameter (Figures 9 and 14) also must be considered. Therefore, an attempt was made to scale bed motion boundaries from one particle size to another, assuming constant particle shape and cylinder diameter, by multiplying the Froude number by a particle-size factor. The ratio of particle diameters raised to the one-half power was found suitable. An example is shown in Figure 15 for Limestone B (dubbed the model material) and Limestone C (called the prototype) in Cylinder A. Similarly, the scaling of bed behavior from one cylinder diameter to another, for the same particle shape and size, was accomplished by modifying the Froude number by the ratio of cylinder diameters raised to the one-half power. Thus the combined scale factor is $(D/d_p)^{1/2}$ and similarity of bed behavior between model and prototype is obtained if

$$[\mathrm{Fr}]_M \left[\frac{D}{d_p}\right]^{1/2}_M = [\mathrm{Fr}]_P \left[\frac{D}{d_p}\right]^{1/2}_P \quad [3]$$

and

$$(\text{pct fill})_M = (\text{pct fill})_P \quad [4]$$

These scaling criteria have been tested by comparing the position of bed motion boundaries of Limestones B, C, and D obtained in Cylinder A (prototype) after modification according to Eq. [3], to the boundaries of Limestone B in

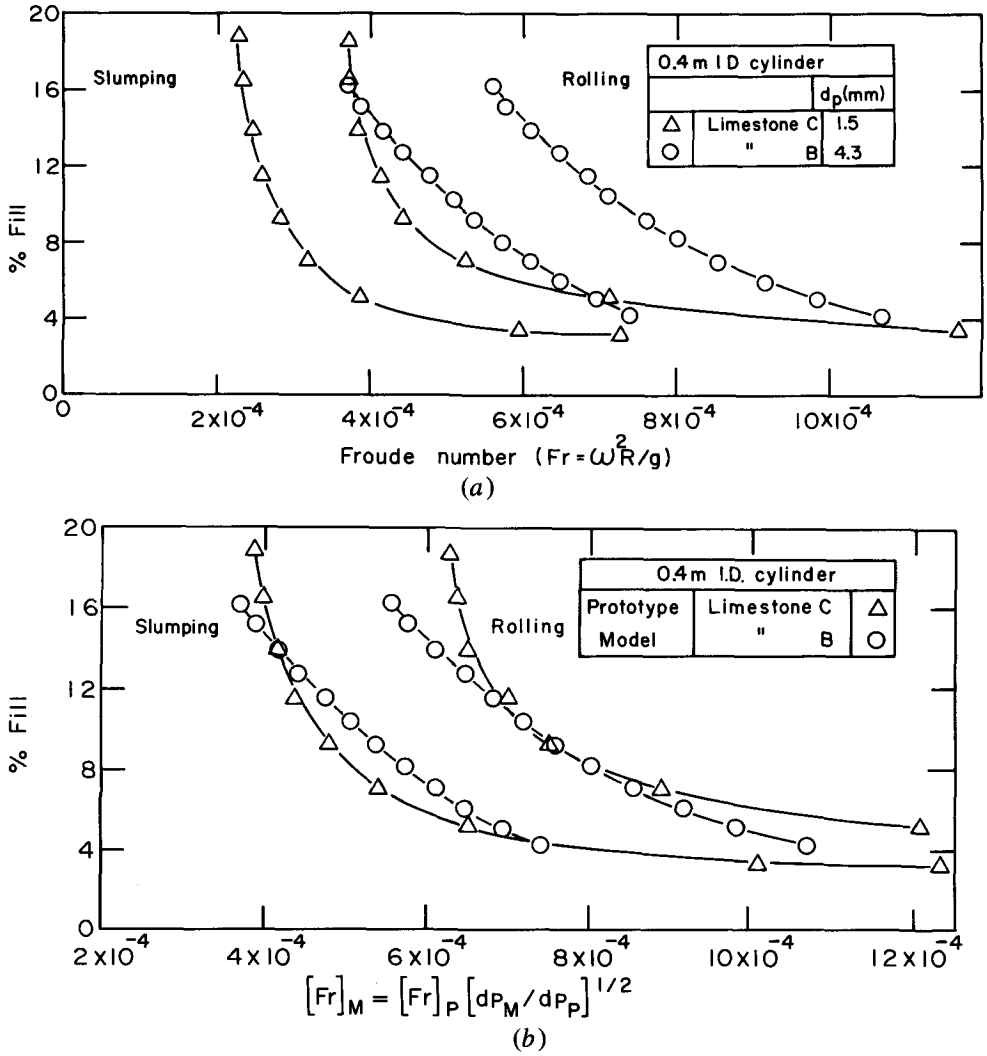


Fig. 15—Dimensionless Bed Behavior Diagrams for Limestones B and C in Cylinder A (*a*) Fr unmodified, (*b*) Fr modified by $(d_{pM}/d_{pp})^{1/2}$.

Cylinder C (model). The results are shown in Figure 16 where the transition zones for all cases are seen to fit within the broad zone of Limestone D obtained in Cylinder A. The transition zones of the other two model cases do not quite overlap with that of the prototype suggesting that a slightly different power in Eq. [3] would be more appropriate. However, the discrepancy, expressed in terms of rotational speed of the larger cylinder, is only 0.15 rpm. It may be noted that the ratio, $D/d_p$, is also a scaling factor in the modeling of the discharge of bulk solids from bins and hoppers,[25] and for slipping in rotary cylinders.[31]

## B. *Characterization of Slumping Beds*

*Maximum Angle of Bed Inclination.* The maximum angle of bed inclination, just prior to a slump, was measured for gravel and Limestone C as a function of rotational speed, and only a slight dependence was found. A linear least-squares fit of the data yielded the following correlation for gravel

$$\phi_U = 0.596n + 40.6 \quad [5]$$

and for Limestone C

$$\phi_U = 1.01n + 37.7 \quad [6]$$

Although the multiple correlation coefficients, having values of 0.342 and 0.599, respectively, were not good, the intercepts of Eqs. [5] and [6] are in excellent agreement with the static angles of repose measured separately (Table I). Part of the reason for the low correlation coefficients is that the maximum angle of bed inclination was never more than 3 deg above the static angle of repose. In addition, the protractor used for the measurements could be read only to the nearest 0.5 deg.

*Shear Angle.* The shear angle was measured for all materials listed in Table I and in the three rotary cylinders. In all cases it was found to be independent of the rotational speed and bed depth, a fact that was used to great advantage in the mathematical modeling study described in the following paper. Values of shear angles measured when the bed was slumping for the different materials and cylinder diameters are presented in Table V. Only a small influence of the latter variable is observed, the shear angle being slightly less in the larger cylinder, particularly for Limestone B. This concurs with results obtained by other workers for the static angle of repose which Brown and Richards have attributed to wall effects.[25] Comparing shear angles of different materials, the effects of particle size and shape are evident. Spherical iron oxide and nickel oxide pellets have lower shear angles than irregularly shaped Limestones B, C, and D. Within each of these two groups of particle shapes, materials with greater particle size have larger shear angles.

**Table V. Shear Angles of Materials in Rotary Cylinders A, B, and C**

| Material | Cylinder Diameter (m) | Shear Angle (Degrees) | Standard Deviation (Degrees) | Number of Observations |
|---|---|---|---|---|
| Gravel | 0.40 | 34.7 | 0.8 | 53 |
| | 1.06 | 34.4 | 0.6 | 26 |
| Iron Oxide | 0.40 | 33.3 | 0.4 | 7 |
| Limestone B | 0.40 | 37.7 | 1.1 | 51 |
| | 1.06 | 34.5 | 0.7 | 39 |
| Limestone C | 0.40 | 33.6 | 0.5 | 37 |
| | 1.06 | 32.5 | 0.8 | 16 |
| Limestone D | 0.40 | 33.5 | 0.3 | 51 |
| Limestone F | 1.06 | 38.5 | 1.2 | 6 |
| Nickel Oxide | 0.40 | 29.9 | 0.7 | 56 |
| Sand A | 0.40 | 32.4 | 0.7 | 5 |
| Sand B | 0.40 | 32.2 | 0.5 | 44 |
| Sand C | 0.40 | 33.0 | — | 1 |

*Slumping Frequency.* The slumping frequency was obtained from the signal of the IR sensor, an example of which was seen in Figure 4, over a time period ranging from 5 to 30 minutes. Figure 17 shows the influence of rotational speed and bed depth on slumping frequency for Limestone B in Cylinder A. Rotational speed has a strong effect, more so at lower speeds, on slumping frequency, but bed depth has

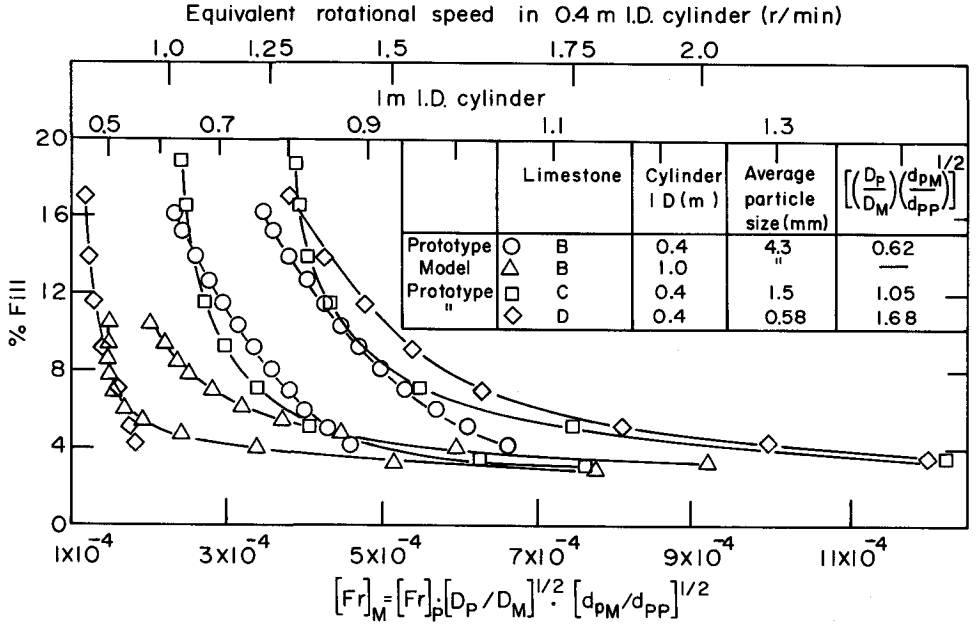


Fig. 16—Dimensionless Bed Behavior Diagrams for Limestones B, C, and D in Cylinders A and C with Froude number modified by ratio of particle size to cylinder diameter.

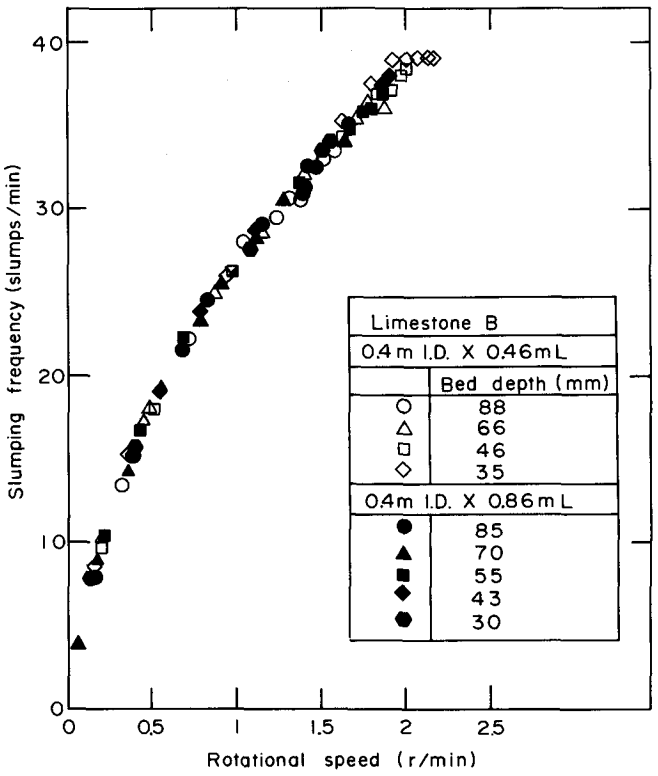


Fig. 17—Slumping frequency as a function of rotational speed for Limestone B in Cylinders A and B showing the effect of bed depth and cylinder length.

no influence. Note that the range of rotational speeds over which slumping measurements can be made decreases with increasing bed depth as shown on the Bed Behavior Diagram (Figure 9). The length of the rotary cylinder has no influence on slumping frequency which indicates that wall effects are negligible. The dependence of slumping frequency on cylinder diameter is shown in Figure 18 for Limestone B. The effect at low rotational speeds, less than 0.3 rpm, is small but above this level, the slumping frequency is lower in the larger cylinder, C. The same results were obtained for Limestone C above 0.75 rpm and for gravel above 0.65 rpm. This effect of diameter is not eliminated by plotting the slumping frequency as a function of the Froude number. This shows again that the Froude number is an insufficient criterion for scaling bed behavior. Figure 19 shows the influence of particle shape and size on slumping frequency. Thus, materials having the same particle shape exhibit an increased slumping frequency with decreasing particle size; and for a constant size the slumping frequency is higher for the particles having the greater sphericity. Clearly then, the slumping frequency of a material is dependent on its physical properties as suggested by Zablotny.[1] Finally, there appears to be a relationship between the order of the slumping frequency plots in Figure 19 and the relative position of the slumping-rolling boundaries seen in Figures 8 through 13 which is more consistent than that observed for the static angle of repose. The higher the slumping frequency curve, the further the bed motion boundaries are shifted to lower rotational speeds in the Bed Behavior Diagrams.

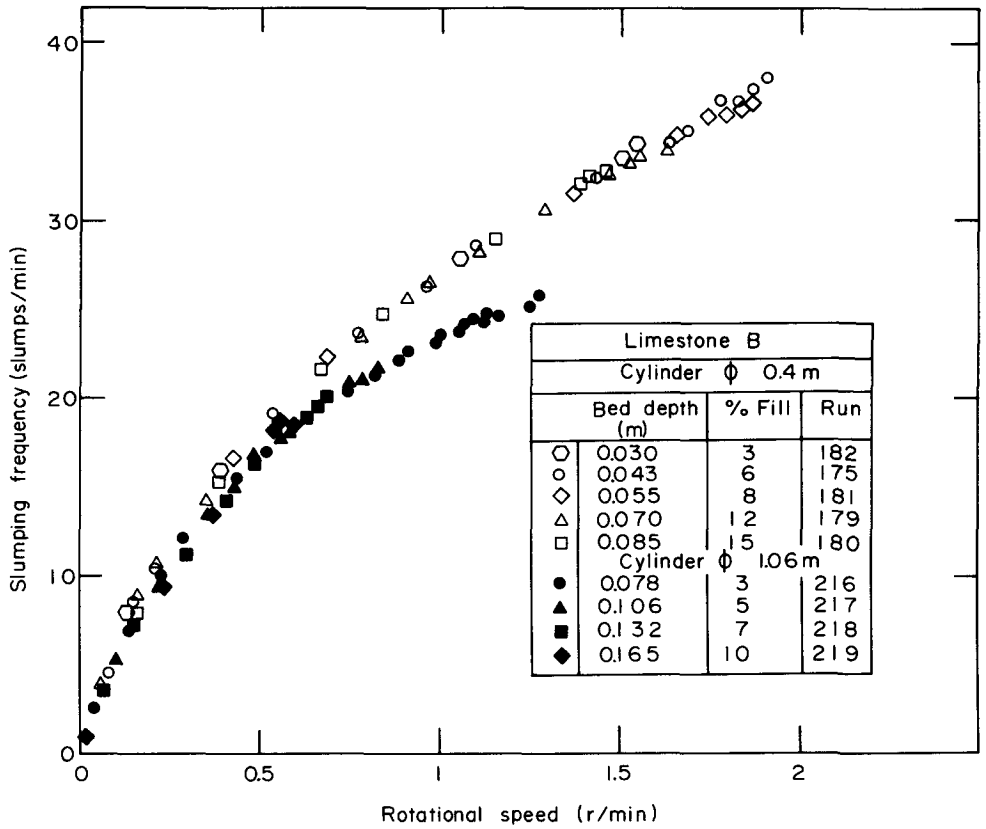


Fig. 18—Slumping frequency as a function of rotational speed for Limestone B showing the effect of cylinder diameter.

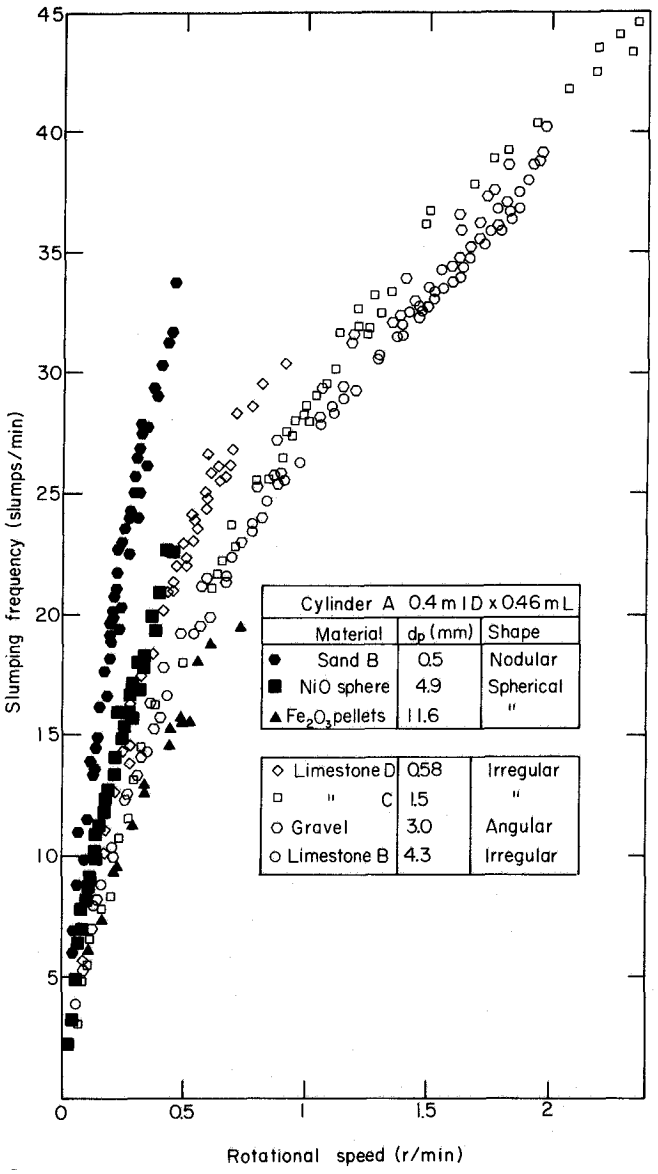


Fig. 19 — Slumping frequency as a function of rotational speed for several materials in Cylinder A showing the effects of particle shape and size.

## C. *Characterization of Rolling Beds*

*Dynamic Angle of Repose.* The dynamic angle of repose was measured at rotational speeds ranging from the slumping-rolling boundary to about 3 rpm and was not affected either by bed depth or rotational speed. Results for the different materials and cylinder diameters are presented in Table VI. The magnitude of the dynamic angle of repose is consistently higher than the shear angle (Table V), but lower than the static angle of repose (Table I). The effects of particle size and shape, and cylinder diameter, on the dynamic angle of repose are similar to those observed earlier with respect to the shear angle. The relative magnitude of the dynamic angles of repose of the different materials are not indicative of their flow properties as reflected by the position of the bed motion boundaries in Figures 8 through 13.

**Table VI. Dynamic Angle of Repose of Materials Tested**

| Material | Cylinder Diameter (m) | Dynamic Angle (Degrees) | Standard Deviation (Degrees) | Number of Observations |
|---|---|---|---|---|
| Gravel | 0.40 | 37.5 | 0.4 | 10 |
| | 1.06 | 37.0 | — | 1 |
| Iron Oxide | 0.40 | 35.2 | 0.3 | 3 |
| Limestone B | 0.40 | 39.6 | 1.3 | 19 |
| | 1.06 | 36.5 | 1.2 | 12 |
| Limestone C | 0.40 | 36.0 | 0.6 | 21 |
| Limestone D | 0.40 | 34.9 | 0.3 | 31 |
| Limestone F | 1.06 | 41.5 | 0.5 | 3 |
| Nickel Oxide | 0.40 | 30.2 | 0.5 | 6 |
| Sand A | 0.40 | 33.8 | 0.9 | 5 |
| Sand B | 0.40 | 33.6 | 0.8 | 41 |
| Sand C | 0.40 | 34.0 | — | 1 |

*Active-Layer Depth.* The active-layer depth was measured by sighting through the plexiglas end plate and using a millimeter scale at the point of maximum thickness of the layer, *i.e.*, where the bed is closest to the center of rotation of the cylinder. The results for different materials are plotted *vs* bed depth in Figure 20. Thus it is seen that at constant bed depth, the active layer is thinner with smaller sized particles. Increasing bed depth and rotational speed individually increase the active-layer thickness. Dividing the active-layer thickness and bed depth by the average particle diameter to obtain the thickness of each zone in terms of number of particles, the data in Figure 20 can be replotted as shown in Figure 21. Then the number of particles through the depth of the active layer is observed to increase with increasing rotational speed and decreasing particle size. From Figure 21, it is also evident that for shallow beds, the active layer may occupy up to one-third of the depth, but for deeper beds ($H/d_p > 50$) this fraction falls off to about 8 pct. Clearly also, as the rotational speed is increased the fraction of particles in the active layer, relative to the passive layer beneath, increases. There is no relationship be-

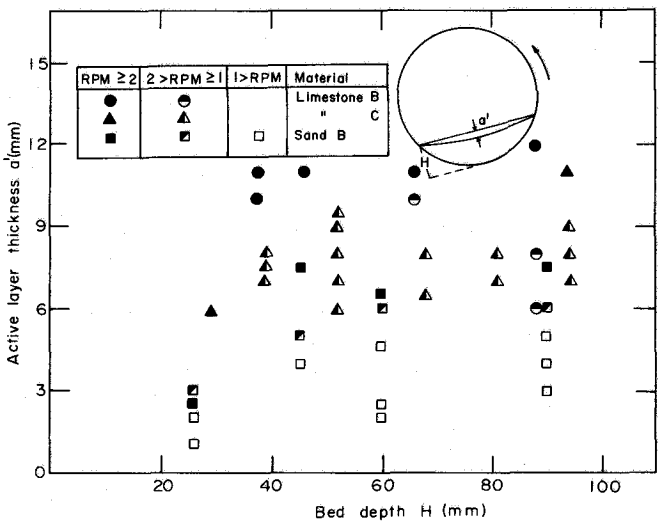


Fig. 20 — Active-layer thickness as a function of bed depth for several materials.

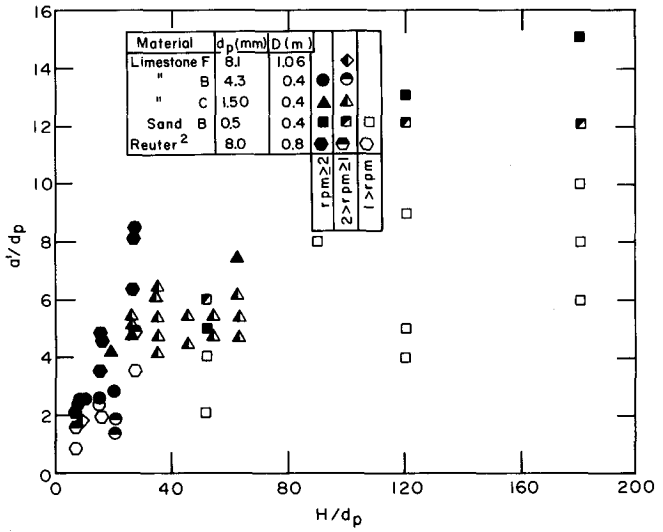


Fig. 21 — Active-layer thickness as a function of bed depth both expressed in terms of number of particles, for several materials.

tween active-layer thickness and bed behavior (Figures 8 through 13), but the active layer may have an important effect on convective heat and mass transfer at the surface of the bed. This is the subject of a current research project.

### D. *Applicability of Results to Design and Operation of Rotary Kilns*

Although the present experiments were carried out at room temperature, the results obtained and approach taken should be applicable generally to rotary kiln processes in which the solids are heated. However, in the latter case it is to be expected that the resulting physical and/or chemical changes experienced by the solids may alter the size, shape, density, or adhesion of particles, thereby affecting transverse bed motion, over the kiln length. Thus, in the case of commercial rotary kilns it may be necessary to determine a different Bed Behavior Diagram for each zone in which solids properties have changed, *e.g.*, drying, calcining, gasification, reduction, *etc.* By reference to these diagrams an operating strategy then may be developed that is compatible with the preferred bed behavior throughout the kiln or in a specific zone of the kiln. This is particularly important with respect to the prevention of slipping beds which are characterized by poor solids mixing and concomitant low heat transfer to the bed. As shown in Figure 5, bed slipping can be eliminated by raising the pct fill, for example, through the introduction of internal dams. Alternatively, the bed-wall friction coefficient could be increased by suitably roughening the wall. Similarly, if a slumping bed is to be avoided in favor of a rolling bed, the pct fill can be increased, particularly at lower solids loadings, or the rotational speed can be raised as shown in Figures 5 to 14.

In designing rotary kilns, the current experimental findings can be applied further to ensure that a given type of bed behavior is avoided or enhanced. Using a kiln of equivalent internal diameter to Cylinder A, a measure of the static angle of repose or the slumping frequency of the solids in the various stages of processing would indicate the slumping-rolling boundary for a kiln of equivalent internal diameter to Cylinder A. Applying Eqs. [3] and [4] would yield the range of rotational speeds required for operating the commercial kiln of a given diameter. With bed behavior in mind, this rotational speed, bed depth, and kiln diameter may then be used to select the remaining kiln design variables (inclination, dams, *etc.*) for a specified throughput and residence time.

It may also be that for a rolling bed the fraction of active layer to the total bed depth, which can be taken from Figures 20 and 21, for example, is an important parameter in the design of new kilns. The greater the fraction of bed occupied by the active layer, the more time particles will be exposed to the hot gases in the freeboard relative to the time spent in the passive region of the bed. This will enhance mixing and as mentioned earlier may increase convective heat transfer to the bed.

## V. SUMMARY

An experimental study of slumping and rolling beds in rotary vessels has revealed the following:

1. Slumping and rolling are uniquely determined by the rotational speed of the cylinder, the bed depth, the cylinder diameter, and the properties of the materials (particle size and shape as manifested in static angle of repose or slumping frequency).
2. For a given material, conditions of slumping and rolling, as well as of slipping, can be represented most conveniently on a Bed Behavior Diagram, *i.e.*, plot of bed depth *vs* rotational speed.
3. Rolling beds are favored by higher pct filling, spherical as opposed to irregularly-shaped particles, smaller particles, materials with a small static angle of repose or high slumping frequency, and larger cylinder diameters.
4. Similarity of bed behavior of materials with the same particle shape but different size and contained in cylinders of different diameter requires that pct fill and $[\mathrm{Fr}] \cdot [D/d_p]^{1/2}$ be maintained constant.
5. In a slumping bed, the maximum angle of bed inclination is only weakly dependent on rotational speed for a given material. The shear angle is independent of the rotational speed and bed depth, and is lower for particles of greater sphericity and smaller diameter.
6. The slumping frequency increases with increasing rotational speed and is greater for more spherical particles and smaller particle sizes. Bed depth has no effect.
7. In a rolling bed, the dynamic angle of repose is not affected by either rotational speed or bed depth, and is lower than the static angle of repose. The dynamic angle of repose is affected by particle characteristics in the same manner as the shear angle.
8. The active-layer thickness in a rolling bed is increased with increasing rotational speed and bed depth. The number of particles through the depth of the active layer increases also with rotational speed and decreasing particle size.

## NOMENCLATURE

| | |
|---|---|
| $a'$ | Active-layer thickness, mm |
| $d_p$ | Particle diameter, mm |
| $D$ | Cylinder diameter, m |
| Fr | Froude number ($= \omega^2 R/g$) |

$g$ Gravitational acceleration, $m/s^2$
$H$ Bed depth, mm
$n$ Rotational speed, rpm
$n_c$ Critical rotational speed for centrifuging, rpm
$R$ Inside radius of cylinder, m
$S$ Slumping frequency, slumps per minute
$t_s$ Slumping time, s
$\varepsilon$ Void fraction of bulk solids
$\phi_R$ Static angle of repose of material, deg
$\phi_U$ Maximum angle of bed inclination in slumping bed
$\rho_B$ Bulk density of solids, $kg/m^3$
$\rho_p$ Particle density
$\mu_{w/s}$ Coefficient of static friction between the cylinder wall and bulk solids
$\omega$ Angular velocity of rotary cylinder, rad per second

Subscripts

$M$ Model
$P$ Prototype

## ACKNOWLEDGMENTS

The authors are grateful to Stelco, Inc. and to the Natural Sciences and Engineering Research Council of Canada for providing financial support in the form of a Stelco Fellowship and Research Assistantship, respectively. Appreciation is also expressed to Mr. E. Sunnergren of Bethlehem Steel, Mr. E. Whitlock of Domtar Chemicals Ltd., and Mr. W. Zimmer of Kennedy Van Saun Corporation for their help and cooperation during the various stages of this project.

## REFERENCES

1. W. W. Zablotny: *Intl. Chem. Eng.*, 1965, vol. 5, pp. 360-66.
2. G. Reuter: Ph.D. Thesis, Rheinisch-Westfälischen Technischen Hochschule Aachen, 1975.
3. W. Schnabel: Ph.D. Thesis, Rheinisch-Westfälischen Technischen Hochschule Aachen, 1977.
4. M. Wahlster, H. G. Jost, H. Serbent, and G. Meyer: *Techn. Mitt. Krupp* (Forsch.-Ber.), 1963, vol. 21, no. 1, pp. 5-14.
5. K. W. Pearce: *J. Inst. Fuel,* 1973, vol. 46, pp. 363-71.
6. G. W. J. Wes, A. A. H. Drinkenburg, and S. Stemerding: *Powder Tech.*, 1976, vol. 13, pp. 177-84.
7. R. Rutgers: *Chem. Eng. Sci.*, 1965, vol. 20, pp. 1079-87.
8. J. J. Ronco: *Industria y Chimica,* 1960, vol. 20, pp. 605-14.
9. F. C. Franklin and L. N. Johanson: *Chem. Eng. Sci.*, 1955, vol. 4, pp. 119-29.
10. A. J. Stepanoff: *Gravity Flow of Bulk Solids and Transportation of Solids in Suspension,* Wiley, Toronto, 1969, pp. 1-21.
11. Y. Oyama: *Rikwagaku-Kenkyo-Jo-Iho Bull.*, 1935, vol. 14, pp. 570-83.
12. E. W. Davis: *Trans. AIME,* 1919, vol. 61, pp. 250-96.
13. K. W. Carley-Macauly and M. B. Donald: *Chem. Eng. Sci.*, 1964, vol. 19, pp. 191-99.
14. J. J. Ronco and M. de Santiago: Universidad Nacional de La Plata, Laboratorio de Ensayo de Materiales e Investigaciones Tecnológicas de la Provincia de Buen Aires (LEMIT), La Plata, República Argentina, unpublished research, 1959.
15. H. E. Rose and R. M. E. Sullivan: *A Treatise on the Internal Mechanics of Ball, Tube and Rod Mills,* Constable and Company Ltd., London, 1957, pp. 35-68 and 201-20.
16. H. E. Rose: *Trans. Inst. Chem. Engrs.*, 1959, vol. 37, pp. 47-64.
17. *Wire Sieves Specification-E-11,* 1970 (Reapproved 1977), 1980 Annual Book of ASTM Standards-Part 13, ASTM, Philadelphia, PA.
18. ASTM Committee E-29, *Manual on Test Sieving Methods,* ASTM Special Technical Publ. 447A (04-447010-23), ASTM, Philadelphia, PA, 1972.
19. R. R. Irani and C. F. Callis: *Particle Size: Measurement, Interpretation and Application,* Wiley, NY, 1963, pp. 34-57.
20. T. Allen: *Particle Size Measurement,* 2nd ed., Chapman and Hall Ltd., London, 1975, pp. 16-43.
21. G. Herdan: *Small Particle Statistics,* 2nd ed., Academic Press Inc., Toronto, 1960, pp. 1-105.
22. *Glossary of Terms Relating to Powders,* British Standard 2955, 1958, Amendment PD 5673, November 1965, SBN: 580 02668X.
23. H. Hausner: *Handbook of Powder Metallurgy,* Chemical Publ. Co. Inc., New York, NY, 1973, pp. 44-48.
24. J. Eastwood, E. J. P. Matzen, M. J. Young, and N. Epstein: *British Chem. Eng.*, 1969, vol. 14, pp. 1542-45.
25. R. L. Brown and J. C. Richards: *Principles of Powder Mechanics,* Pergamon Press, Toronto, 1970, pp. 1-115.
26. J. K. Brimacombe and A. P. Watkinson: *Metall. Trans. B,* 1978, vol. 9B, pp. 201-08.
27. F. Von Conrad, E. Cremer, and Th. Kraus: *Radex-Rundschau,* 1951, vol. 6, pp. 227-33.
28. J. C. Richards, editor: *The Storage and Recovery of Particulate Solids,* The Institution of Chemical Engineers, London, 1966, pp. 1-5, 39-56, and 91-94.
29. H. B. Sutherland and D. F. Neale: *Acta Technica Academiae Scientiarum Hungaricae,* 1968, vol. 63, pp. 297-313.
30. H. E. Rose and G. D. Blunt: *Proc. Instu. Mech. Engrs.*, 1956, vol. 170, pp. 793-800.